# Second-Order Effects on Wind-Induced Structural Behavior of High-Rise Steel Buildings

Sejun Park[1] and DongHun Yeo, M.ASCE[2]

**Abstract:** This paper investigates second-order effects on wind-induced structural dynamic behavior of a 60-story high-rise steel structure known as the Commonwealth Advisory Aeronautical Research Council (CAARC) building model. These effects are considered in the structural analysis by using a geometric stiffness method allowing the dynamic analysis to be performed without iterations. Data sets of the aerodynamic pressure on the CAARC building model for suburban exposure are used in the database-assisted design (DAD) procedure to calculate, in addition to overturning moments and shear forces at the base, members' demand-to-capacity indexes (DCIs), interstory drift ratios, and resultant accelerations. Dynamic analyses are performed using four reference mean hourly wind speeds at the rooftop for suburban terrain exposure ($U_{ref} = 20$ and 40 m/s for serviceability analysis, and 60 and 80 m/s for strength analysis). The second-order effects decrease natural frequencies of vibration of the building by up to 12%. In the strength analysis with $U_{ref} = 80$ m/s, second-order effects increase nondirectional peak global responses by up to 15% for overturning moments, 9% for base shears, and 10% for torsional moments. The responses of 21 members selected in this study are increased by up to 19% for columns, 41% for beams, and 31% for diagonal bracings in the case of the DCIs for the interaction of axial forces and bending moments ($B_{ij}^{PM}$) and by up to 67% for columns, 26% for beams, and 13% for diagonal bracings in the case of the DCIs for the shear forces ($B_{ij}^{V}$). In the serviceability analysis with $U_{ref} = 40$ m/s, second-order effects increase the interstory drift ratios by up to 17% and the resultant accelerations at the top floor by up to 2%. This case study shows that the second-order effects can considerably affect not only drift control but also the design of members for strength. **DOI: 10.1061/(ASCE) ST.1943-541X.0001943.** 

**Author keywords:** Commonwealth Advisory Aeronautical Research Council (CAARC) building; Database-assisted design (DAD); Demand-to-capacity index (DCI); Geometric stiffness approach; High-rise steel structures; Second-order effects; Wind effects.



## Introduction

In high-rise buildings gravity loads cause an amplification of the structural system's displacements and moments induced by lateral loads. The amplification is a second-order effect that includes both the $P$-$\Delta$ effect due to member chord rotation and the $P$-$\delta$ effect due to member curvature. High-rise buildings, which typically have fundamental frequencies of vibration lower than 1 Hz, tend to be more susceptible to second-order effects associated with wind than with seismic loads because wind loads are generally characterized by low frequencies while seismic loads usually have higher frequency content. Therefore, controlling second-order effects of high-rise buildings subjected to the wind loading is necessary from a perspective of both strength design and serviceability. Two basic approaches to assessing dynamic instability induced by secondary effects on multistory buildings have been developed to date: (1) second-order elastic analysis with geometric nonlinearities, and (2) second-order inelastic analysis with geometric and material nonlinearities.

Within the framework of the second-order elastic analysis, several methods have been proposed. The additional story shear force method, which deals only with the $P$-$\Delta$ effect approximately, implements additional story shears due to the vertical loads with regard to the deformed geometry of the structure, and subsequent reanalysis should be performed iteratively (Wood et al. 1976). The moment amplification method [also known as the B1/B2 approach introduced in ANSI and AISC (2010b) and LeMessurier (1976, 1977)], which involves the calculation of B1 (for $P$-$\delta$) and B2 (for $P$-$\Delta$), is simple and fast, and is for this reason commonly used in design practice. However, the approximations it entails may be unsatisfactory in some cases. The fictitious column method proposed by Rutenberg (1981) considers the secondary effect by using a fictitious member having negative lateral stiffness properties proportional to the story weights. This fictitious member reduces the lateral stiffness of the structure so that the drifts and moments of members can be functions of the lateral loads and the gravity loads.

As computational capabilities have advanced, comprehensive matrix analysis approaches have been developed. These approaches can reliably account for both $P$-$\Delta$ and $P$-$\delta$ effects by employing stability functions or geometric stiffness formulations (Goto and Chen 1987; White and Hajjar 1991). If stability functions are used, the governing differential equations of a beam-column element are solved iteratively by updating the stiffness matrix and the force vector due to the secondary effects (Al-Mashary and Chen 1990). In the geometric stiffness formulation, an assumed cubic polynomial shape function is employed to solve the governing equations; this is computationally more advantageous than the use of stability functions, while the error generally remains less than 1% (Allen and Bulson 1980, p. 276).

Among second-order inelastic analyses, the pushover analysis has been widely used. For simplicity, the inelastic material behavior

[1]Postdoctoral Research Fellow, Engineering Laboratory, National Institute of Standards and Technology, Gaithersburg, MD 20899. ORCID: https://orcid.org/0000-0003-4617-8771. E-mail: sejun.park@nist.gov

[2]Research Engineer, Engineering Laboratory, National Institute of Standards and Technology, 100 Bureau Dr., Gaithersburg, MD 20899 (corresponding author). E-mail: donghun.yeo@nist.gov

Note. This manuscript was submitted on October 27, 2016; approved on July 13, 2017; published online on December 8, 2017. Discussion period open until May 8, 2018; separate discussions must be submitted for individual papers. This paper is part of the ***Journal of Structural Engineering***, © ASCE, ISSN 0733-9445.

is typically assumed to be bilinear with zero postyield stiffness (i.e., elastic-perfectly plastic). Several nonlinear dynamic analysis techniques for multiple- or equivalent single-degree-of-freedom systems are then applied to estimate the inelastic dynamic responses. Bernal (1998), MacRae (1993), Tremblay et al. (2001), Gupta and Krawinkler (2000), and Humar et al. (2006) carried out inelastic dynamic analyses on various models of multistory buildings designed for seismic loads and proposed several methods of accounting for the secondary effects. They reported that the second-order effects typically result in an increase of the response over the first-order response by approximately 10–25%, depending on the lateral forces resisting system, the number of stories, and the magnitude and duration of ground motions.

Second-order effects on tall buildings have been extensively investigated for the case of seismic loads (e.g., Gupta and Krawinkler 2000; Humar et al. 2006; MacRae 1993; Williamson 2003). However, research for the case of wind loads has been much more limited. The ASCE Task Committee on Drift Control of Steel Building Structures (1988) has suggested such research. Analytical studies have, therefore, been performed on steel frames subjected to wind to assess second-order effects on lateral drift of structures as they affect serviceability (Baji et al. 2012; Berding 2006). However, these studies did not include second-order effects on structural strength.

The main objective of this paper is to study the second-order effects on the wind-induced strength and serviceability behavior of a high-rise steel structure. This study adopted the geometric stiffness approach and used this approach in conjunction with the database-assisted design (DAD) technique to account for secondary effects on dynamic structural responses under wind with various speeds and directions. The structural system was assumed to behave linearly (i.e., material nonlinearity is not considered). That approach was applied in a case study of a 60-story building, known as the Commonwealth Advisory Aeronautical Research Council (CAARC) building model, in suburban exposure, for which the wind load was based on aerodynamic pressure data sets obtained in wind tunnel tests. First- and second-order responses were evaluated for overturning moments and base shear forces, members' demand-to-capacity indexes (DCIs), interstory drift ratios, and accelerations.

## Database-Assisted Design Procedure Accounting for Second-Order Effects

### Geometric Stiffness Approach for Second-Order Elastic Analysis

In second-order elastic analyses of both $P$-$\Delta$ (member chord rotation effects) and $P$-$\delta$ (member curvature effects), static equilibrium is formulated on the deformed configuration of the structure. The secondary effects can be accounted for by using a matrix known as the geometric stiffness matrix (also called initial stress stiffness matrix) (Wilson and Habibullah 1987). For the frame analysis, the geometric stiffness matrix represents the stiffening and weakening effect by the tensile (positive) and compressive (negative) load in the structural member, respectively. The second-order problem can be formulated and solved without iterations as a linear system where the geometric stiffness matrix is subtracted from the elastic stiffness matrix, as expressed in Eq. (1)

$$\mathbf{F} = [\mathbf{K} - \mathbf{K_G}]\mathbf{\Delta} \tag{1}$$

where $\mathbf{F}$ = applied static lateral force matrix; $\mathbf{K}$ = elastic stiffness matrix; $\mathbf{\Delta}$ = element nodal displacement vector; and $\mathbf{K_G}$ = geometric stiffness matrix, which accounts for second-order moments caused by the interaction of the gravity loads and lateral deflections of structure.

In the geometric stiffness method, (1) if the initial axial loads in the elements are significantly modified by the application of external loads, iterative calculations may be required; and (2) if $P/P_e$ exceeds 0.4, where $P_e = \pi^2 EI/L^2$, the corresponding members must be subdivided into two or more elements to limit the errors in the stiffness matrix; this is associated only with the $P$-$\delta$ amplification (White and Hajjar 1991). This solution is as accurate as the exact solution obtained by a matrix approach based on stability functions (Al-Mashary and Chen 1990).

The matrix equation of dynamic equilibrium in a structural system can also be formulated as

$$\mathbf{M}\ddot{\mathbf{\Delta}}(\mathbf{t}) + \mathbf{C}\dot{\mathbf{\Delta}}(\mathbf{t}) + [\mathbf{K} - \mathbf{K_G}]\mathbf{\Delta}(\mathbf{t}) = \mathbf{F}(t) \tag{2}$$

where $\mathbf{M}$, $\mathbf{C}$, and $\mathbf{F}(t)$ = mass, damping, and external excitation matrices at time $t$, respectively. Because the lateral stiffness of the structural system is effectively reduced by $\mathbf{K_G}$, the natural frequencies of vibration will be lowered and their mode shapes will be slightly changed in comparison with those of the analysis ignoring the secondary effects. These lower frequencies and the corresponding mode shapes represent the actual free vibration responses of the structure under the second-order influence (Newmark and Rosenblueth 1971). Based on the dynamic properties resulting from Eq. (2), the DAD procedure can evaluate the structural responses to wind and perform the design procedure of a high-rise building by considering the second-order effects under wind excitation.

### Overview of the DAD Procedure

Fig. 1 illustrates the DAD procedure considering the second-order effects on a high-rise building. The procedure within dotted lines represents the main algorithm of the *HR_DAD* software. The natural frequencies of vibration and mode shapes including the second-order effects can be obtained in a modal analysis from a finite-element analysis program, and are input into the main algorithm of the DAD for considering the second-order effects. In the modal analysis the factored dead and live loads should be used as vertical loads (White and Hajjar 1991), and separate analysis should be required for each factored load combination [as shown in Eqs. (3) and (4)] for second-order analysis. In the DAD module, dynamic analyses are performed for the building model with a lumped mass on each floor to which gravity and wind loads are applied. The wind loads at the floors' mass centers are calculated from aerodynamic pressures on the building based on a set of wind speeds and wind directions of interest. The outputs of the dynamic analyses consist of (1) time series of internal forces on three cross sections of each member obtained from effective lateral and torsional loads on floors multiplied by an influence coefficient matrix, and (2) time series of displacements and accelerations on floors. These results are converted to design parameters, such as DCIs for each structural member, the interstory drift ratios in the principal directions of the structure, and resultant accelerations at corners of the top floor. Demand-to-capacity indexes of a structural member indicate the interaction of the ratios of the internal forces on the member to the measures of the member's corresponding nominal capacities [for details, see Section 19.4 in Simiu (2011) and NIST Technical Note 1940 (Park and Yeo 2016)]. The influence coefficient matrix in the seconder-order analysis is calculated from the structure with the reduced stiffness [Eq. (1)]. For design purposes, the peak of the time series of each DCI is used and can be efficiently calculated using the multiple points-in-time (MPIT)

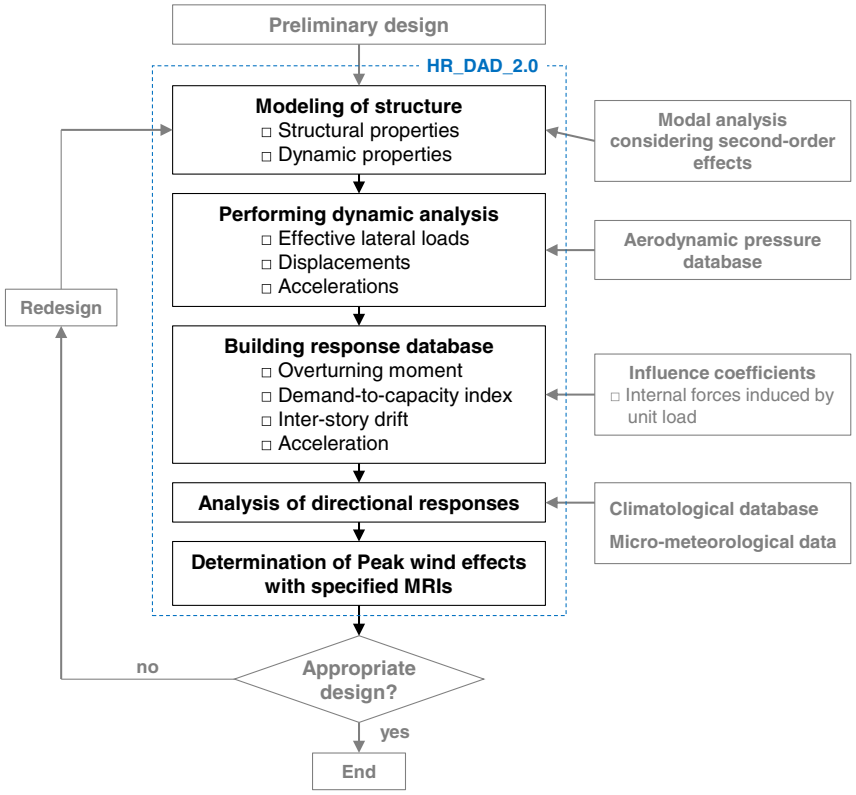


**Fig. 1.** Overview of DAD procedure

approach (Yeo 2013). This study uses 30 peaks of individual wind effects (Yeo 2011). Directional wind effects are calculated by using directional wind speed climatological databases (hurricane and/or nonhurricane data sets) (Yeo 2011). The peak wind effects with a specified mean recurrence interval (MRI) of, e.g., 700 or 1,700 years, are estimated using a nonparametric statistical method [for details, see Section 12.4 in Simiu (2011)].

## Case Study

Fig. 2 depicts the 60-story high-rise steel structure being considered, with 182.88-m height, 45.72-m width, and 30.48-m depth, known as the CAARC building, studied by various researchers (Melbourne 1980; Simiu et al. 2008; Venanzi 2005). Wind direction is defined by the clockwise angle $\theta$, with the positive $x$-axis parallel to the long dimension, and the $y$-axis parallel to the short dimension, of the rectangular cross section of the building. The building has an outrigger system to resist the lateral load similar to the structural system studied by Simiu et al. (2008) that consists of 2,100 columns, 3,480 beams, and 2,560 diagonal bracings. Columns and beams are classified into three types as corner, external, and core for columns, and external, internal, and core for beams, respectively. Diagonal bracings are divided into two types as core and outrigger bracings. Each type of structural member (column, beam, bracing member) has the same dimensions for 10 successive floors of the building's 60 floors. The columns and bracings have hollow structural sections (HSS) and the beams have a rolled W-sections, selected from the *Steel Construction Manual* (ANSI and AISC 2010a). The mass density of the building is 237 $\mathrm{kg/m^3}$. The yield strength of steel for all members is 250 MPa. The modal damping ratios are assumed to be 1.5% in all modes considered in this study.

The building is assumed to have suburban terrain exposure. Time series of aerodynamic loads on each floor are calculated from the pressure data with wind directions in 10° increments measured from wind tunnel experiments at the Prato, Italy, Inter-University Research Centre on Building Aerodynamics and Wind Engineering (CRIAC IV-DIC) Boundary Layer Wind Tunnel (Venanzi 2005).

Under the assumption of linear elastic structural behaviors, dynamic analyses of the building were carried out from the viewpoints of two design categories, i.e., serviceability and strength, and each has different load combinations associated with gravity and wind loads based on a range of wind speeds depending on the nominal wind load stated in ASCE 7-10 (2010). Two load combination cases [LC1 and LC2 in Eq. (3)] were employed for strength design (ASCE 2010, Section 2.3) and one [LC3 in Eq. (4)] was employed for serviceability design (ASCE 2010, Commentary Appendix C)

$$1.2D + 1.0L + 1.0W(\mathrm{LC1}) \quad \text{and} \quad 0.9D + 1.0W(\mathrm{LC2}) \tag{3}$$

$$1.0D + 0.5L + 1.0W(\mathrm{LC3}) \tag{4}$$

where $D$ = dead loads; $L$ = live loads; and $W$ = wind loads.

### *Dynamic Properties and Modal Contribution*

Once initial dimensions of members in the building were obtained, the modal analysis was conducted with and without the second-order effects to calculate the corresponding natural frequencies and mode shapes using *SAP 2000*. Fig. 3 and Table 1 show the mode shapes and the associated natural frequencies up to the sixth mode of the building, respectively. The first mode corresponds to drift along the $y$-axis, the second to drift along the $x$-axis, and the third to rotation along the $z$-axis. The following fourth, fifth, and sixth modes correspond to the second mode of the $y$-direction

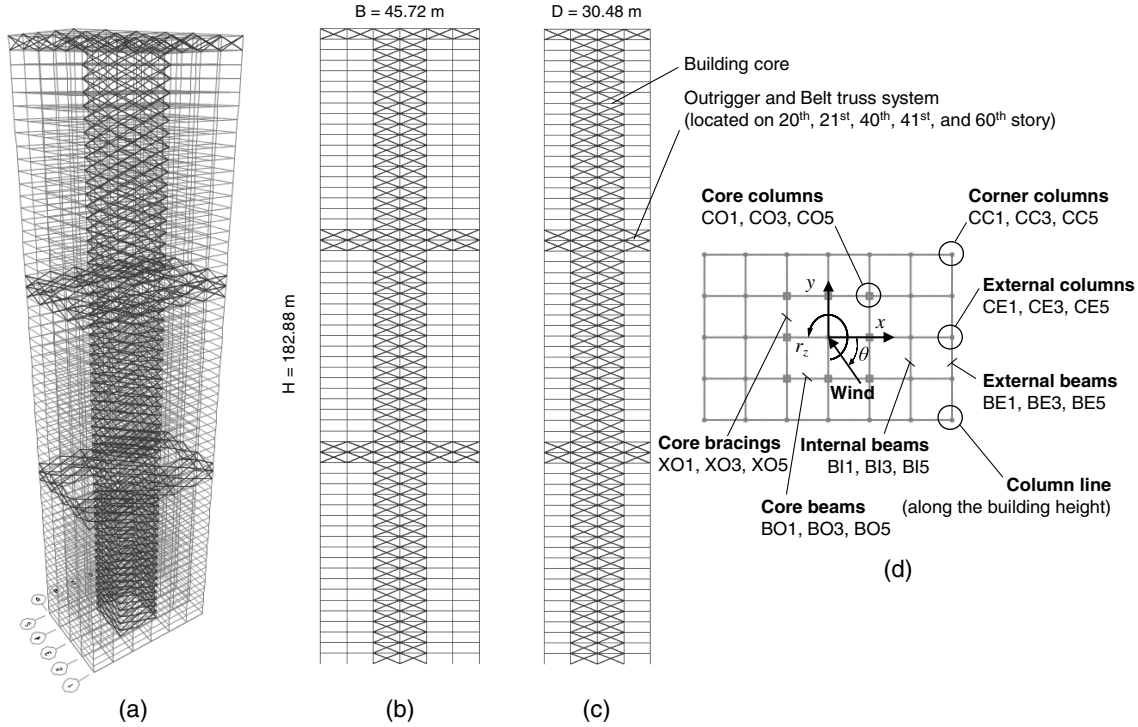


**Fig. 2.** Schematic views of structural system and selected members: (a) three-dimensional view; (b) front view; (c) side view; (d) plan view and selected members and column lin ($\theta$ = wind direction)

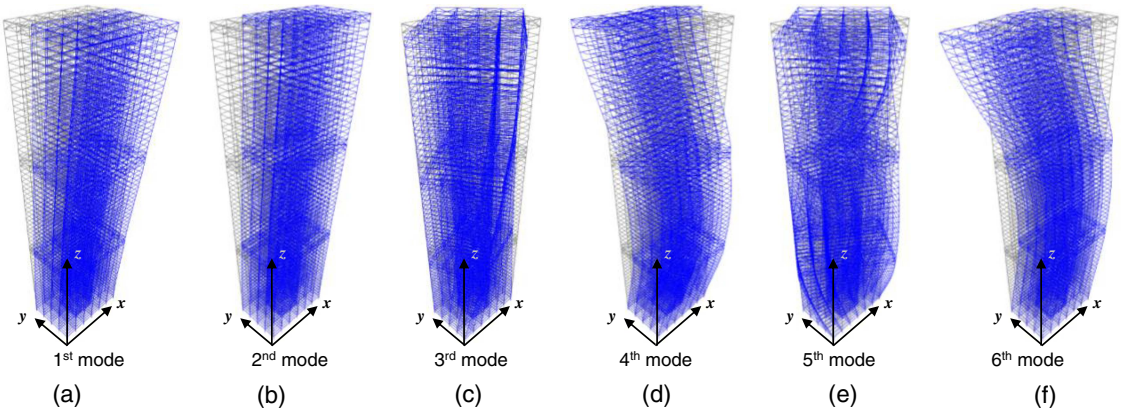


**Fig. 3.** First six mode shapes: (a) first mode: first translation mode in $y$-direction; (b) second mode: first translational mode in $x$-direction; (c) third mode: first rotational mode in $z$-direction; (d) fourth mode: second translation mode in $y$-direction; (e) fifth mode: second rotational mode in $z$-direction; (f) sixth mode: second translational mode in $x$-direction

translational motion, the rotational motion, and the $x$-direction translational motion, respectively. As expected, the natural frequencies of vibration are lower in the analysis with the second-order effects than in one without the effects because the lateral stiffness ($[\mathbf{K}]$) in the second-order analysis was reduced effectively by the geometric stiffness ($[\mathbf{K_G}]$) composed of gravity loads and story height. As shown in Table 1, the second-order effects decrease the natural frequencies of the building by up to 12%.

For the investigation of modal contributions to structural responses to wind, dynamic analyses by the *HR_DAD* algorithm based on the modal superposition method were performed with 12 accumulated mode cases from the first mode up to the 12th mode (i.e., first, first to second, ..., first to 12th). For example, for the resultant top-floor acceleration at a building corner, Fig. 4 represents the ratios of the peak resultant accelerations with and without second-order effects in accumulated mode cases to those without the effects in the modes up to 12th mode. The accelerations were calculated at a corner of the top floor under a mean hourly wind speed of 60 m/s with $\theta = 90°$. As shown in the figure, the

**Table 1.** Dynamic Properties of Building with and without Second-Order Effect

| Analysis type | First | Second | Third | Fourth | Fifth | Sixth |
|---|---|---|---|---|---|---|
| Natural frequencies (Hz) | | | | | | |
| First order (A) | 0.165 | 0.174 | 0.188 | 0.503 | 0.505 | 0.516 |
| Second order (B) | 0.154 | 0.164 | 0.165 | 0.478 | 0.484 | 0.498 |
| Ratio (B/A) | 0.93 | 0.94 | 0.88 | 0.95 | 0.96 | 0.97 |

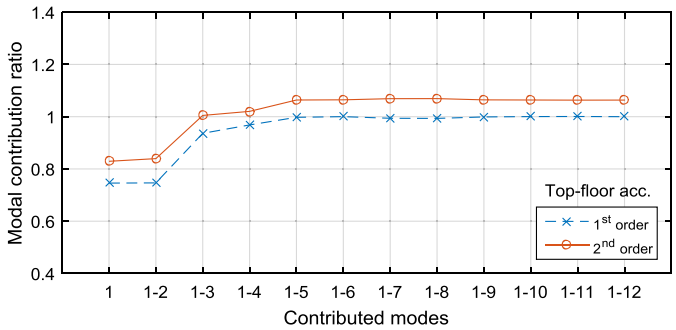


**Fig. 4.** Accumulated modal contributions to resultant top-floor accelerations

acceleration ratios without second-order effects are 0.74 for the first two modes, and 0.93, 0.96, 0.99, and 1.00 for the first three, four, five, and six modes. A similar trend is shown in the analysis with second-order effects, except for an approximately 7% increase of their magnitudes in comparison with the analysis without second-order effects. These results imply that it is reasonable to use the first six modes in the modal superposition analysis for accurately assessing the dynamic responses of the high-rise building model to wind, with or without second-order effects.

### *Dynamic Responses Considering Second-Order Effect*

Dynamic analyses under LC1 [Eq. (3)] were performed using four reference wind speeds ($U_{ref} = 20$, 40, 60, and 80 m/s; mean hourly wind speeds at the rooftop of the building with suburban terrain exposure). These wind speeds can be converted to 3-s gust wind speeds at 10-m elevation over open terrain exposure resulting in approximately $U_{design} = 22$, 43, 65, and 87 m/s, respectively. The first two wind speeds ($U_{ref} = 20$ and 40 m/s) were selected for serviceability design analysis because they correspond to typical ASCE-based basic wind speeds with MRI up to 25 years (ASCE 2010, Figs. CC-1 to CC-2), and the last two wind speeds ($U_{ref} = 60$ and 80 m/s) were chosen for strength design analysis because they are as high as the basic wind speeds for Occupancy Category III and IV buildings with MRI up to 1,700 years (ASCE 2010, Fig. 26.5-1B). The basic wind speed for Occupancy Category IV buildings near Miami is approximately 90 m/s corresponding to MRI = 3,000 years in ASCE 7-16 (ASCE 2016). Though the wind directions considered in this study are $\theta = 0°$–$350°$ in increments of 10°, for reasons of symmetry only directions from $\theta = 0°$–$90°$ need to be used.

The second-order effects on the overturning moment in the along-wind and the across-wind directions were investigated. The effective overturning moment and the wind-induced overturning moments were calculated by summing up moments at the base induced by the effective force and by the wind force alone, acting at all floors.

Fig. 5 shows the spectral densities of the along-wind and across-wind overturning moments at wind speeds $U_{ref} = 20$, 60, and 100 m/s with wind direction $\theta = 90°$. Although the probability of attaining a 100-m/s wind speed is not considered in current building codes, this speed is included in this study to illustrate the major increase in the response due to the coincidence or near-coincidence of the vortex-shedding frequency and one of the natural frequencies of the building. The secondary horizontal axes representing the reduced frequencies for each wind speed are also included in the figure. The dim gray and gray areas represent the effective overturning moments in the analyses without and with second-order effects, respectively, and the light gray area indicates the wind-induced overturning moments induced by the wind forces alone. In the case of along-wind overturning moments [Figs. 5(a), (c), and (e)], background responses are noticeable, especially at $U_{ref} = 20$ m/s. The effective overturning moments show peak along-wind responses at the lowest natural frequencies ($n_1^{1st}$ and $n_1^{2nd}$ for the first-order and the second-order analyses, respectively) of the building.

As shown in Figs. 5(b), (d), and (f), which represent across-wind overturning moments induced by wind with direction $\theta = 90°$, as the wind speed increases the vortex shedding frequency gets closer to the natural frequency of the building. Resonance occurs in the response with second-order effects at the wind speed $U_{ref} = 100$ m/s [Fig. 5(f)] when the vortex shedding frequency is close to the second and the third natural frequencies (≈0.165 Hz). These two frequencies are almost identical in the second-order analysis (Table 1). This explains why the across-wind overturning moment in the $y$-direction increases significantly when the 100-m/s wind is acting on the building along the $y$-direction.

Fig. 6 shows the second-order effects on the overturning moment coefficient. The along- and across-wind peak overturning moments are shown as functions of wind speed $U_{ref}$ and wind direction $\theta$

$$C_{Mx}(U_{ref},\theta) \quad \text{or}$$
$$C_{My}(U_{ref},\theta) = \frac{M_{ovtn,x}(U_{ref},\theta) \text{ or } M_{ovtn,y}(U_{ref},\theta)}{\frac{1}{2}\rho U_{ref}^2 BH^2} \tag{5}$$

where $M_{ovtn,x}$ and $M_{ovtn,y}$ = overturning moments in the $x$- and $y$-directions, respectively; $\rho$ = air density; $U_{ref}$ = reference wind speed at the rooftop of the building; $B$ = wide dimension of the building; and $H$ = height of the building. In the case of the 0° wind direction [Fig. 6(a)], the along-wind moment coefficients are more or less constant, regardless of wind speeds; one possible reason that the along-wind moment coefficients are not exactly constant is that the ordinate of the spectral density of the along-wind flow fluctuations corresponding to the natural frequency of the structure is a function of wind velocity. This introduces a nonlinear effect in the response. The across-wind moment coefficients generally increase with wind speeds, but have a peak at 90 m/s, especially in the second-order analysis, where the dominant frequency of the across-wind aerodynamic force in the $y$-direction is close to the first natural frequency of vibration of the building with second-order effects.

In the case of the 90° wind direction [Fig. 6(b)], the along-wind moment coefficients are approximately independent of wind speeds and the across-wind ones significantly increase from 80 m/s and have the peak at 100 m/s, where the dominant frequency of the wind force in the across-wind ($x$) direction is close to the second natural frequency of vibration, particularly for the second-order analysis.

The second-order effects are investigated on base shear force coefficients ($C_{Fx}$ and $C_{Fy}$) and overturning moment coefficients ($C_{Mx}$ and $C_{My}$) in the $x$- and $y$-directions, respectively, and torsional moment coefficient ($C_T$) at the base of the structure. The shear force and torsional moment coefficients at the base are defined as

$$C_{Fx}(U_{ref},\theta) \quad \text{or}$$
$$C_{Fy}(U_{ref},\theta) = \frac{F_x(U_{ref},\theta) \text{ or } F_y(U_{ref},\theta)}{\frac{1}{2}\rho U_{ref}^2 BH} \tag{6}$$

$$C_T(U_{ref},\theta) = \frac{T_z(U_{ref},\theta)}{\frac{1}{2}\rho U_{ref}^2 BH^2} \tag{7}$$

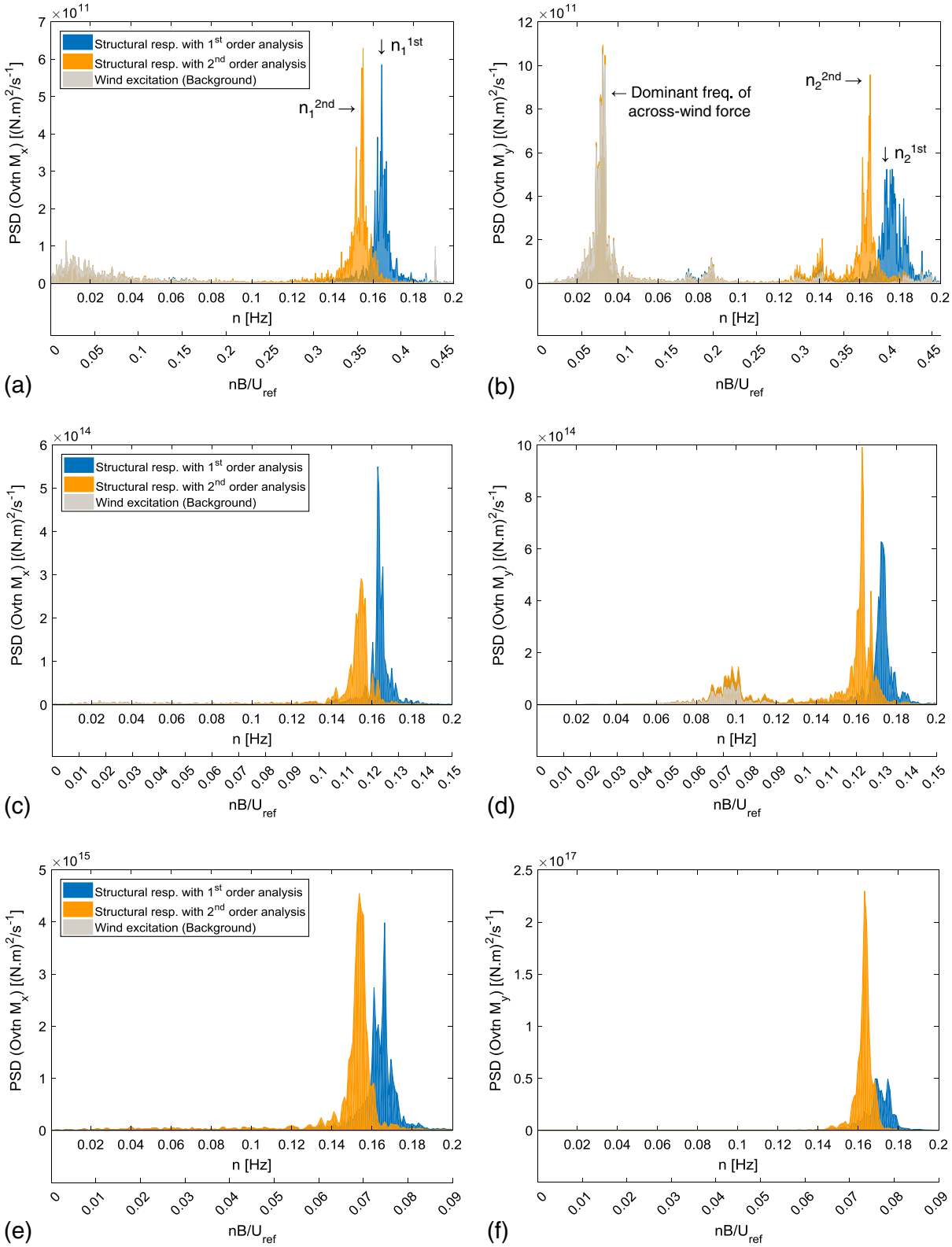


**Fig. 5.** Frequency distributions of wind excitation and responses with respect to hourly mean winds at the rooftop: (a) along-wind response with $U_{ref} = 20$ m/s; (b) across-wind response with $U_{ref} = 20$ m/s; (c) along-wind response with $U_{ref} = 60$ m/s; (d) across-wind response with $U_{ref} = 60$ m/s; (e) along-wind response with $U_{ref} = 100$ m/s; (f) across-wind response with $U_{ref} = 100$ m/s; secondary horizontal axis: reduced frequency $= nB/U_{ref}$, where $n$ is frequency, $B$ is building width of 45.72 m, and $U_{ref} = U_H$

where $F_x$ and $F_y$ = base shear forces in the $x$- and $y$-directions, respectively; and $T_z$ = base torsional moment in the $z$-direction. Figs. 7 and 8 show those shear force and torsional moment coefficients at the base as a function of wind direction in the wind speed of $U_{ref} = 60$ m/s, respectively. The symbols represent the mean values of force and moment coefficients and the bars crossing these symbols indicate a range from their minimum to maximum peak values. The directions at which the along-wind responses occur are

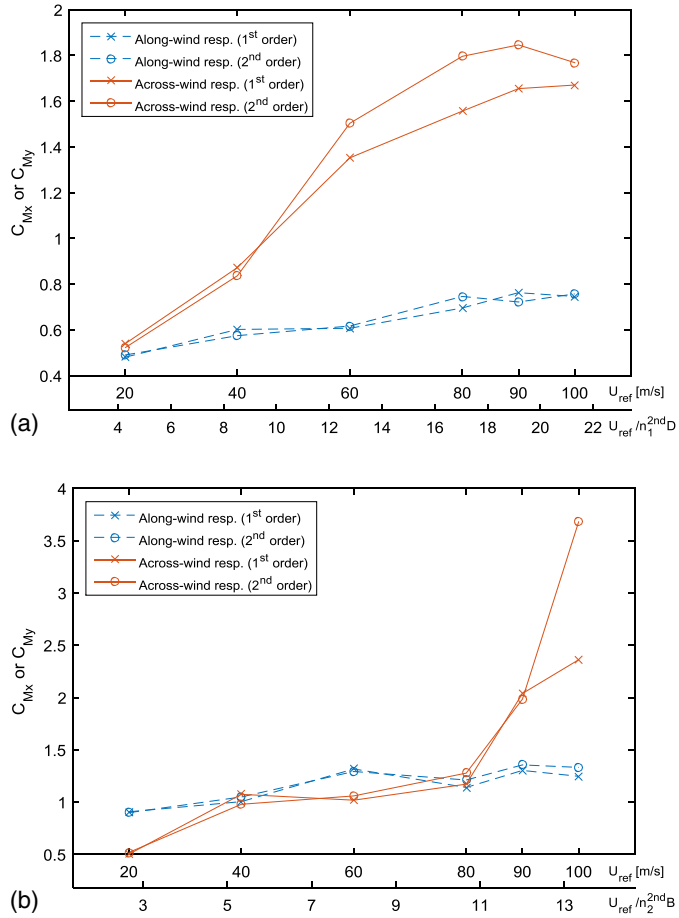


**Fig. 6.** Peak effective overturning moment coefficients under along- and across-wind responses ($n_1^{1\text{st}}$ and $n_1^{2\text{nd}}$ represent the first- and the second-mode natural frequencies of building in the second-order analysis, respectively; $D = 30.48$ m, $B = 45.72$ m): (a) wind direction of 0°; (b) wind direction of 90°

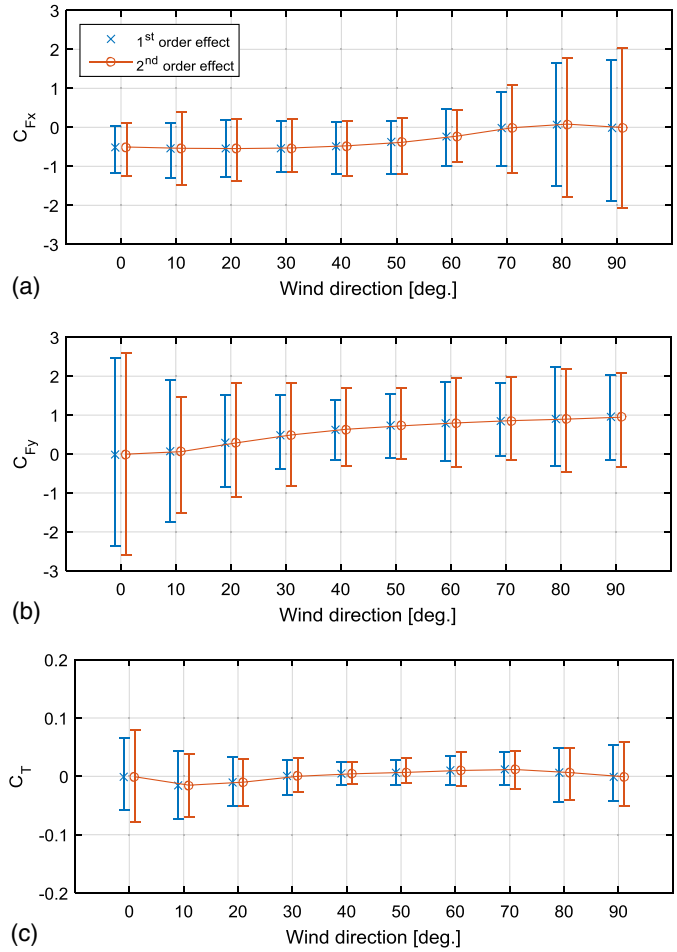


**Fig. 7.** Force coefficients as a function of wind direction ($U_{\text{ref}} = 60$ m/s): (a) $C_{Fx}$; (b) $C_{Fy}$; (c) $C_T$

0° for $C_{Fx}$ and 90° for $C_{My}$. Those at which the across-wind responses occur are 90° for $C_{Fy}$ and 0° for $C_{Mx}$. The results show no second-order effects on the mean values, but differences in peak values, which are of more interest from a viewpoint of structural design. The across-wind shear forces and overturning moment fluctuations are stronger than their along-wind counterparts. This is due to the across-wind vortex-induced wind forces. The fluctuations with second-order effects are larger in most cases, especially when the wind directions are aligned with the principal axes of the building (i.e., $\theta = 0°$ and 90°). In addition, the torsional moments have the largest negative and positive mean values at $\theta = 10°$ and 70° because one separation point is shifted from a leading edge to a trailing edge of the structure while the other separation point is not changed, as also observed by Matsumoto et al. (1998). Wind-induced torsional responses will be significant when a building has the cross-section center at each floor offset from its elastic center.

Table 2 summarizes the effects of secondary action on nondirectional peak base shear, torsional, and overturning moments based on the reference wind speeds under LC1. The peak values in the table are defined as the largest of all directional peak values (i.e., the largest of all directional peak values calculated from all wind directions). From a practical design viewpoint, it is reasonable to use the nondirectional peak values for assessing the second-order effects. As shown in the table, the second-order effects are

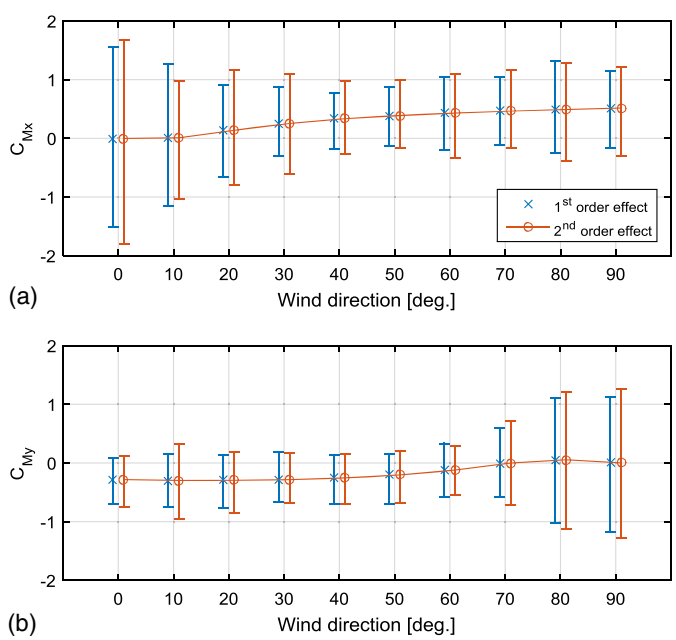


**Fig. 8.** Moment coefficients as a function of wind direction ($U_{\text{ref}} = 60$ m/s): (a) $C_{Mx}$; (b) $C_{My}$

**Table 2.** Second-Order Effects on the Peak Base Shear, Torsional, and Overturning Coefficients, Regardless of Wind Directions

| Coefficient | Reference wind speeds ($U_{ref}$) under LC1 | | | | | | | |
|---|---|---|---|---|---|---|---|---|
| | 20 m/s | | 40 m/s | | 60 m/s | | 80 m/s | |
| $C_{Fx}$ | 0.98[a] | 0.94[b] | 0.91 | 1.62 | 1.08 | 1.71 | 1.09 | 2.06 |
| | | 0.96[c] | | 1.77 | | 1.58 | | 1.89 |
| $C_{Fy}$ | 1.02 | 1.73 | 0.92 | 1.89 | 1.03 | 2.24 | 1.06 | 2.60 |
| | | 1.70 | | 2.06 | | 2.18 | | 2.46 |
| $C_{Tz}$ | 0.92 | 0.04 | 1.11 | 0.06 | 0.99 | 0.07 | 1.10 | 0.08 |
| | | 0.05 | | 0.05 | | 0.07 | | 0.07 |
| $C_{M,x}$ | 1.00 | 0.92 | 0.89 | 1.05 | 1.11 | 1.50 | 1.15 | 1.80 |
| | | 0.92 | | 1.18 | | 1.35 | | 1.56 |
| $C_{M,y}$ | 1.03 | 0.52 | 0.91 | 0.98 | 1.04 | 1.06 | 1.09 | 1.28 |
| | | 0.50 | | 1.07 | | 1.02 | | 1.17 |

[a]Ratio of peak nondirectional base shear or moment with second-order effect to the counterpart with first-order effect (b/c).
[b]Peak base shear or moment coefficient with second-order effect.
[c]Peak base shear or moment coefficient with first-order effect.

generally on the order of 10–15% of the first-order effects at wind speeds.

### Strength Design: Demand-to-Capacity Index

Response databases of demand-to-capacity indexes were calculated in the two load combination cases [LC1 and LC2 in Eq. (3)] for 21 selected structural members: nine columns, nine beams, and three diagonal bracings [Fig. 2(d)] consisting of (1) three core columns (CO1, CO3, CO5), three corner columns (CC1, CC3, CC5), and three external columns (CE1, CE3, CE5), on the 1st, 21st, and 41st stories; and (2) three external beams (BE1, BE3, BE5), three internal beams (BI1, BI3, BI5), and three core beams (BO1, BO3, BO5), on the 10th, 30th, and 50th floors, and three core bracings (XO1, XO3, XO5) on the 1st, 21st, and 41st stories. Their DCIs for interaction of axial forces and bending moments ($B_{ij}^{PM}$) and for shear forces ($B_{ij}^{V}$) were calculated with wind directions ($\theta = 0°, 10°, \ldots, 350°$) and wind speeds ($U_{ref} = 60$ and 80 m/s). Fig. 9 shows an example of the response databases of $B_{ij}^{PM}$ and $B_{ij}^{V}$ for the corner column at the first story (CC1) under LC1. The details of the DCIs for the steel members are provided in the NIST Technical Note 1940 (Park and Yeo 2016).

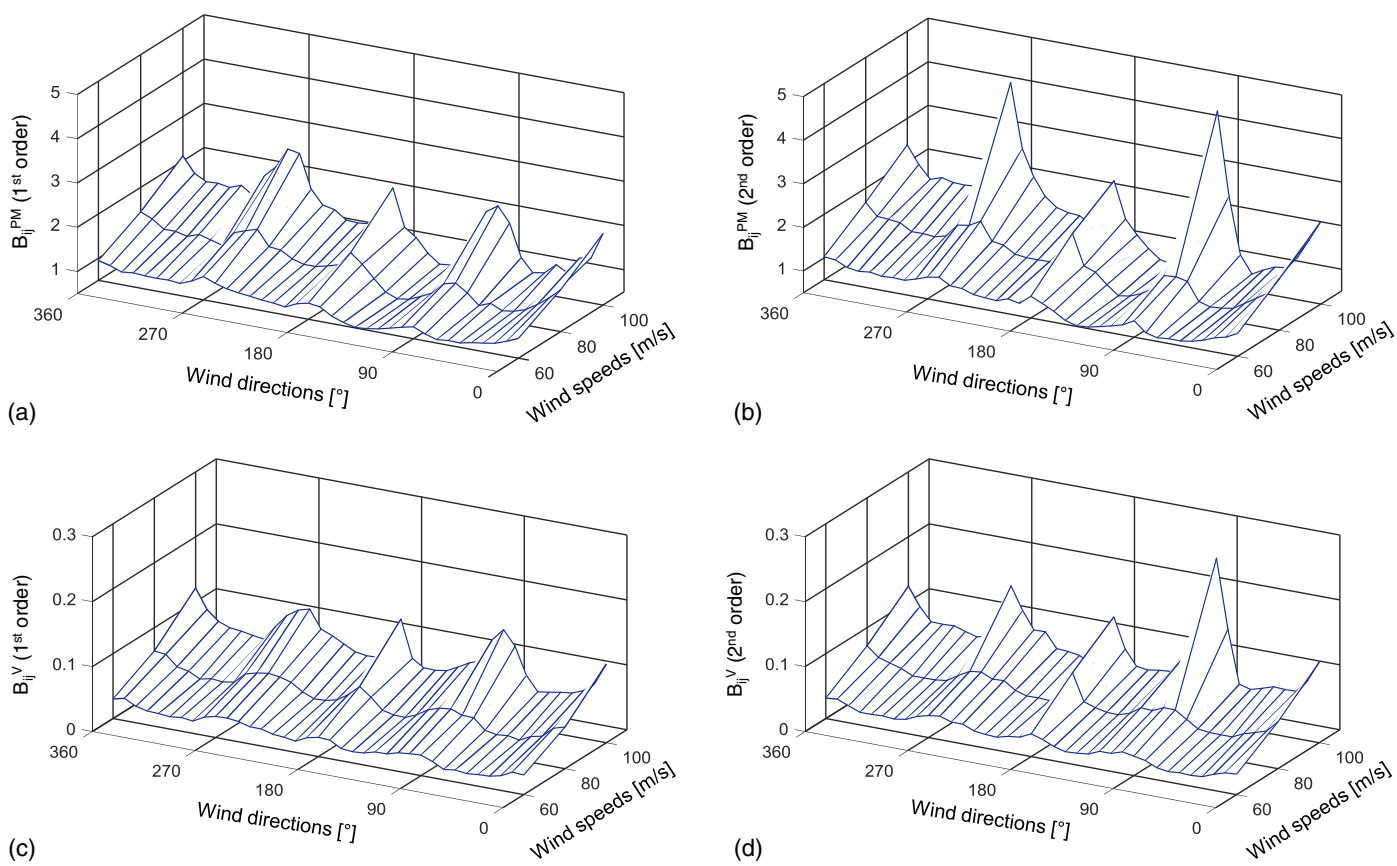


**Fig. 9.** Response databases: $B_{ij}^{PM}$ and $B_{ij}^{V}$ (member label = CC1): (a) $B_{ij}^{PM}$ with first-order effect; (b) $B_{ij}^{PM}$ with second-order effect; (c) $B_{ij}^{V}$ with first-order effect; (d) $B_{ij}^{V}$ with second-order effect

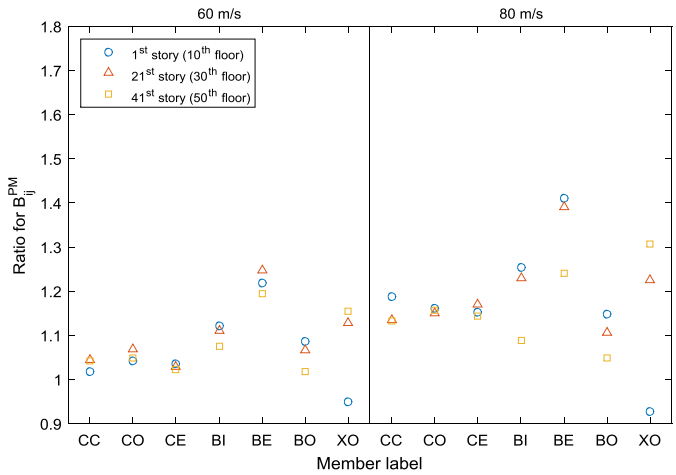


**Fig. 10.** Second-order effect ratios for $B_{ij}^{PM}$ depending on members' labels and wind speeds

Figs. 10 and 11 illustrate the second-order effect ratios, which are the larger value of ratios of peak nondirectional DCIs for the selected members with a second-order effect to counterpart with a first-order effect, in LC1 and LC2, respectively. Overall, the maximum $B_{ij}^{PM}$ values are larger in LC1 than in LC2, but the maximum $B_{ij}^{V}$ values in LC1 are as high as those in LC2. Most of the peak $B_{ij}^{PM}$ values are over unity, and they are even higher than 9 for a certain wind speed. This is due not only to use of consistent structural members of the building under various wind speeds, but also to the limitations of the elastic analysis performed in this study. As shown in the figures, the second-order effects on axial loads and moments (i.e., $B_{ij}^{PM}$) of all columns are less than 7% for $U_{ref} = 60$ m/s. However, they increase by approximately 20% for $U_{ref} = 80$ m/s. In the case of $B_{ij}^{PM}$ for beams, the second-order effects increase by up to 40% for external, internal, and core beams (BE, BI, and BO) for all reference wind speeds.

The demand-to-capacity indexes for shears, $B_{ij}^{V}$, were much lower than $B_{ij}^{PM}$ in all cases; all the $B_{ij}^{V}$ were less than 0.5. The second-order effects on all columns increase with wind speeds: up to 48 and 67%, respectively, for $U_{ref} = 60$ and 80 m/s. In the case of beams, the second-order effects are up to 26% in all wind speeds. The $B_{ij}^{V}$ values of most members are considerably smaller than the $B_{ij}^{PM}$, which means $B_{ij}^{V}$ is not the critical factor in the structural design of the building considered in this study.

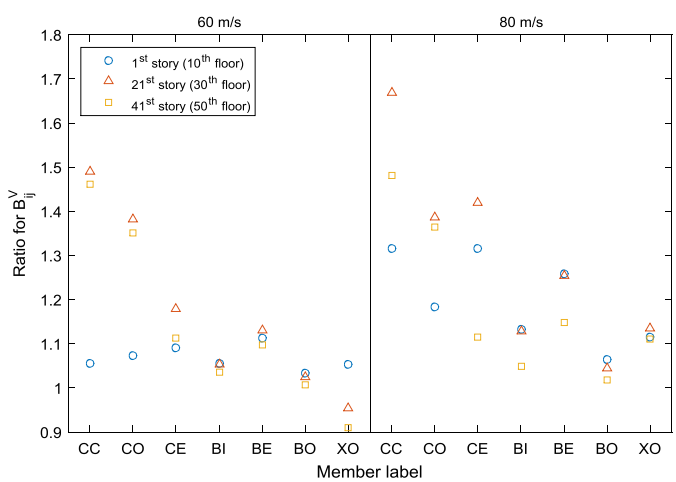


**Fig. 11.** Second-order effect ratios for $B_{ij}^{V}$ depending on members' labels and wind speeds

### *Serviceability Design: Interstory Drift and Acceleration*

Response databases for interstory drift ratios and accelerations were calculated in the load combination case of LC3 [Eq. (4)] along a column line of interest for serviceability design [Fig. 2(d)]. The reference wind speeds were taken as 20 and 40 m/s for the analysis for serviceability. Details on expressions for the interstory drift ratio and the acceleration for the building are provided in the NIST Technical Note 1940 (Park and Yeo 2016). Fig. 12 shows the interstory drift ratios in both the $x$- and $y$-directions corresponding to the across- and the along-wind response, respectively, along the selected corner column line [Fig. 2(d)] when the reference wind speed is $U_{ref} = 40$ m/s and the wind direction is $\theta = 90°$. The peak along-wind interstory drift ratios are $27.4 \times 10^{-4}$ at the 42nd story in the first-order analysis and $35.2 \times 10^{-4}$ at the 24th story in the second-order analysis, and the peak across-wind ones are $29.3 \times 10^{-4}$ at the 28th story in the first-order analysis and $33.6 \times 10^{-4}$ at the 29th story in the second-order analysis. Thus, the second-order effect increases the interstory drifts by up to 30 and 17% in the along- and across-wind response, respectively. The interstory drift ratios are less than 0.001 on the 20th, 21st, 40th, and 41st stories, where the outrigger and belt truss systems are located. Fig. 13 plots the peak interstory drift ratios from all stories as a function of wind direction. Because the selected column line is located at the lower right-hand corner of the building plane [Fig. 2(d)], the peak interstory drifts for the $x$- and $y$-directions are symmetry with the wind directions of 90° and 270° in Fig. 13(a) and with 180° in Fig. 13(b), respectively. As shown in the figures, the peak interstory drift ratios in the $x$-direction are $29.3 \times 10^{-4}$ in the first-order analysis and $33.6 \times 10^{-4}$ in the second-order

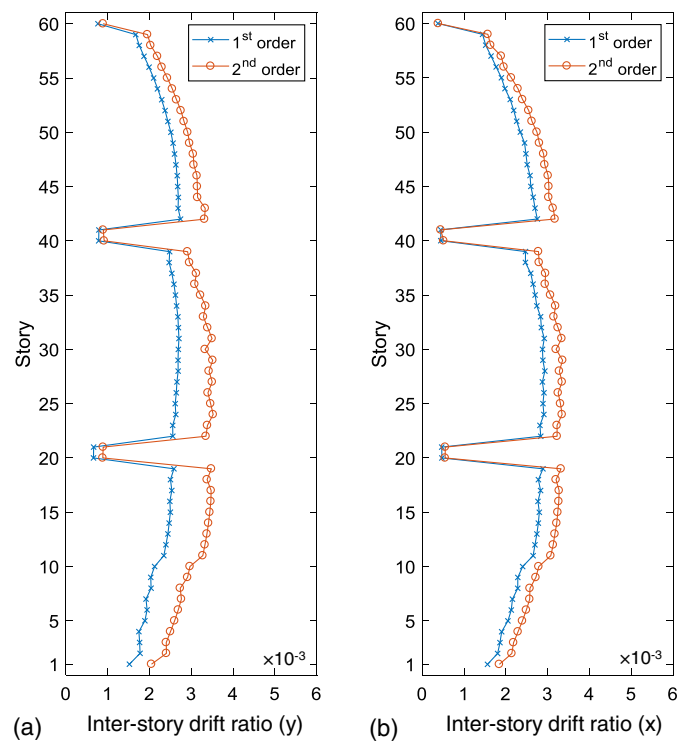


**Fig. 12.** Interstory drifts along the selected column line ($U_{ref} = 40$ m/s, $\theta = 90°$): (a) along-wind response ($y$-direction); (b) across-wind response ($x$-direction)

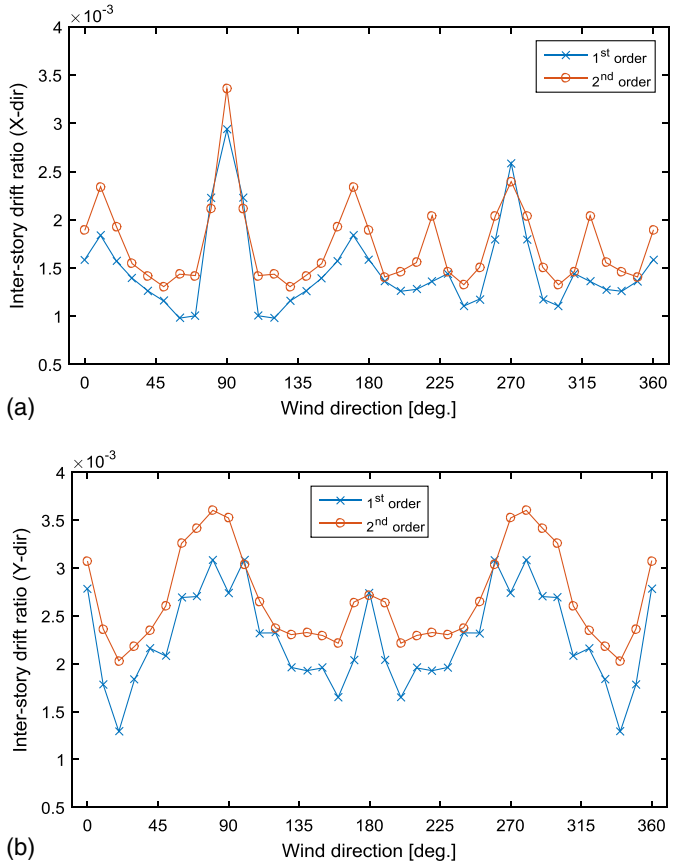


**Fig. 13.** Peak interstory drifts with respect to wind directions (at the selected column line; $U_{ref} = 40$ m/s): (a) $x$-direction; (b) $y$-direction

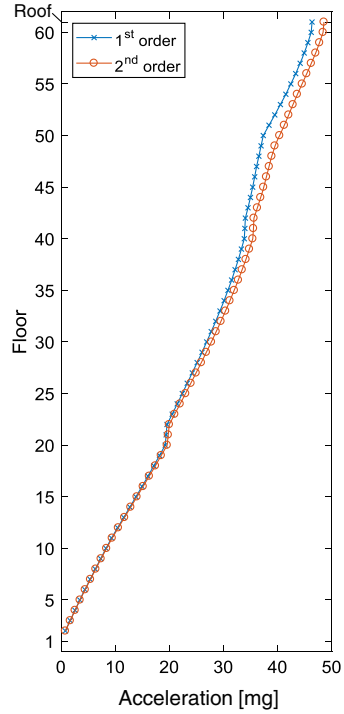


**Fig. 14.** Resultant accelerations for the selected column line ($U_{ref} = 40$ m/s, $\theta = 90°$)

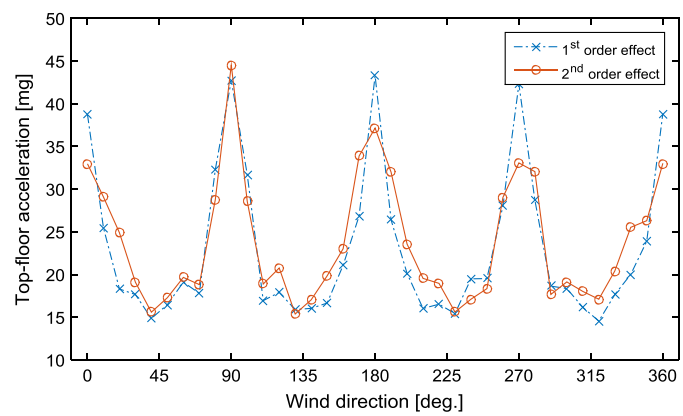


**Fig. 15.** Peak top-floor accelerations with respect to wind directions (at the selected column line; $U_{ref} = 40$ m/s)

analysis when the wind direction is 90° (i.e., across-wind response). The counterparts in the $y$-direction are $30.9 \times 10^{-4}$ in the first-order analysis and $36.0 \times 10^{-4}$ in the second-order analysis when wind is approaching at 80°. The $y$-direction interstory drift ratio at wind direction of 80° is larger than that of 90°, which can be explained by the reattachment of wind flows on the rectangular section of the building as previously mentioned in "Dynamic Responses Considering Second-Order Effect." This behavior is also observed in the $x$-direction interstory drift ratios for wind directions of 0° and 10°.

Figs. 14 and 15 show the resultant accelerations for the selected column line [Fig. 2(d)] at the wind direction of 90° and the top-floor accelerations with respect to wind directions, respectively, when the reference wind speed is 40 m/s. The unit of acceleration used in the figures is milli-$g$, where $g$ is the gravitational acceleration (9.81 m/s$^2$). As shown in Fig. 14, the second-order effect can be noticeable only above approximately the top-half floors and increases the top-floor acceleration by 2%.

Table 3 summarizes the second-order effects on peak interstory drift ratios and resultant accelerations of the selected column line [Fig. 2(d)] as a function of reference wind speeds. The peak values in the table are defined in a manner similar to the peak base shears and overturning moments (Table 2) as the largest of all directional peak interstory drift ratios and acceleration values calculated from all wind directions. Based on the results in this case study, the second-order effects increase the interstory drift ratios by up to 14–21% and the resultant accelerations by up to approximately and 2–6%. When the reference wind speed increases from 20 to 40 m/s, the second-order effects on interstory drift ratios of the building become more significant than those on base shears

**Table 3.** Second-Order Effects on the Peak Interstory Drift Ratios and Resultant Accelerations

| Serviceability factors | Reference wind speed ($U_{ref}$) under LC3 | | | |
|---|---|---|---|---|
| | 20 m/s | | 40 m/s | |
| In-dr. ratio in $x$ | 1.21[a] | $4.6 \times 10^{-4}$[b] | 1.14 | $33.6 \times 10^{-4}$ |
| | | $3.8 \times 10^{-4}$[c] | | $29.3 \times 10^{-4}$ |
| In-dr. ratio in $y$ | 1.17 | $7.7 \times 10^{-4}$ | 1.17 | $36.0 \times 10^{-4}$ |
| | | $6.6 \times 10^{-4}$ | | $30.9 \times 10^{-4}$ |
| Resultant acceleration (milli-$g$) | 1.06 | 5.37 | 1.02 | 44.50 |
| | | 5.06 | | 43.53 |

Note: In-dr. = inter-story drift.
[a]Ratio of peak serviceability factors with second-order effect to the counterpart with first-order effect.
[b]Peak serviceability factors with second-order effects.
[c]Peak serviceability factors with first-order effects.

and overturning moments. This can be explained by a simple expression

$$\frac{\mathbf{F}_{eff,i}^{2\text{nd}}}{\mathbf{F}_{eff,i}^{1\text{st}}} = \frac{\mathbf{F}_{aero,i} - \mathbf{M}\ddot{\boldsymbol{\Delta}}_i^{2\text{nd}}}{\mathbf{F}_{aero,i} - \mathbf{M}\ddot{\boldsymbol{\Delta}}_i^{1\text{st}}} = \frac{\mathbf{K}_i^{2\text{nd}}\boldsymbol{\Delta}_i^{2\text{nd}}}{\mathbf{K}_i^{1\text{st}}\boldsymbol{\Delta}_i^{1\text{st}}} \tag{8}$$

where $\mathbf{F}_{eff}$ = effective force matrix (i.e., aerodynamic + inertial force) associated with base shears and overturning moments; $\mathbf{F}_{aero}$ = aerodynamic force matrix; $\mathbf{M}$ = mass matrix; $\mathbf{K}$ = stiffness matrix; $\boldsymbol{\Delta}$ = displacement matrix; $\ddot{\boldsymbol{\Delta}}$ = acceleration matrix; the subscript $i$ = directions of each factor (translational $x$ and $y$, and rotational $z$); and the superscripts 1st and 2nd = analysis types (with or without second-order effects). From this expression, it follows that the displacement ratio ($\boldsymbol{\Delta}_i^{2\text{nd}}/\boldsymbol{\Delta}_i^{1\text{st}}$) is directly proportional to the effective force ratio multiplied by the reciprocal of the stiffness ratio ($\mathbf{K}_i^{2\text{nd}}/\mathbf{K}_i^{1\text{st}}$), where $\mathbf{K}^{2\text{nd}} = \mathbf{K}^{1\text{st}} - \mathbf{K}_G$. The stiffness ratio can be estimated by the square of the natural frequency ratio, $(n_n^{2\text{nd}}/n_n^{1\text{st}})^2$. Because the stiffness ratio is less than unity, the displacement ratio will be larger than the effective force ratio.

## Conclusions

This paper presents an investigation into second-order effects on the wind-induced structural dynamic behavior of a high-rise steel structure, as considered within a DAD context. A geometric stiffness method that accounts for second-order effects and allows the dynamic analysis to be performed without iterations is shown to be applicable in conjunction with DAD and was used in a study of the response of a 60-story building, known as the CAARC building. Data sets of the aerodynamic pressure on the CAARC building for suburban exposure were used to calculate overturning moments and shear forces at the base, as well as members' DCIs, interstory drift ratios, and resultant accelerations. Under the assumption of linear elastic structural behavior, dynamic analyses of the building were performed for serviceability and strength. The structural behavior was analyzed using global effects (overturning moments, base shear forces, and torsion), as well as local effects: (1) for strength design, DCIs of structural members; (2) for serviceability design, interstory drift ratios, and resultant accelerations along a column line. Those values were obtained both by considering and disregarding wind directional effects. Of four reference wind speeds at the rooftop of the building ($U_{ref} = 20$, 40, 60, and 80 m/s), the first two were used for serviceability analysis, and the last two for strength analysis. The following conclusions can be drawn from this study:

- The second-order effects decrease natural frequencies of vibration of the building by up to 12%. As a result, the second and the third natural frequencies become close to less than 1%. The first six modes in the modal superposition analysis were shown to be sufficient for accurately assessing the dynamic responses, both when considering and when disregarding second-order effects.
- For nondirectional second-order effects, the peak base shears are increased by up to 9%, the torsional moments by up to 10%, and the overturning moments by up to 15%, in the case of $U_{ref} = 80$ m/s.
- For secondary effects on strength of structural members, the DCIs for axial force and bending moments ($B_{ij}^{PM}$) are increased by up to 19% for columns, 41% for beams, and 31% for diagonal bracings, and those for shear forces ($B_{ij}^{V}$) by up to 67% for columns, 26% for beams, and 13% for diagonal bracings, in the case of $U_{ref} = 80$ m/s. The $B_{ij}^{V}$ values of most members are considerably smaller than the $B_{ij}^{PM}$, which means $B_{ij}^{V}$ is not a critical factor in the structural design of the building considered in this study.
- The second-order effects increase the interstory drift ratios by up to 17% and the resultant accelerations by up to 2% in the 40-m/s wind speed. The interstory drift ratios show the secondary effects along all stories except ones where the outrigger and belt truss systems are located. However, the secondary effects on the resultant acceleration are shown above approximately the top-half floors.

While much research was performed on secondary effects on a high-rise building subjected to earthquake loads, this work is, to the authors' knowledge, the first study to focus on the systematic analysis of second-order effects on high-rise buildings subjected to wind loads. This case study shows that the second-order effects can considerably affect not only drift control but also the design of members for strength. However, those effects will differ from structure to structure because the response of a high-rise structure to wind depends strongly upon the building shape, the dynamic characteristics of the structural system, and the turbulence produced in the atmospheric boundary layer by the nature of the terrain surface. Additional studies on second-order effects are therefore in order. However, the methodology presented and illustrated in this paper is typically applicable to structures that differ in various ways from the structure considered herein.

## Acknowledgments

The wind tunnel data developed at the CRIAC IV-DIC Boundary Layer Wind Tunnel were kindly provided by Dr. Ilaria Venanzi of the University of Perugia. Dr. Emil Simiu served as project leader and provided helpful comments.

## References

Allen, H. G., and Bulson, P. S. (1980). *Background to buckling*, McGraw-Hill, Berkshire, U.K.

Al-Mashary, F., and Chen, W. F. (1990). "Elastic second-order analysis for frame design." *J. Constr. Steel Res.*, 15(4), 303–322.

ANSI (American National Standards Institute) and AISC. (2010a). *Steel construction manual*, 14th Ed., Chicago.

ANSI (American National Standards Institute) and AISC. (2010b). "Specifications for structural steel buildings." *AISC 360-10*, Chicago.

ASCE. (2010). "Minimum design loads for buildings and other structures." *ASCE 7-10*, Reston, VA.

ASCE. (2016). "Minimum design loads for buildings and other structures." *ASCE 7-16*, Reston, VA.

ASCE Task Committee on Drift Control of Steel Building Structures. (1988). "Wind drift design of steel-framed buildings: State-of-the-art report." *J. Struct. Eng.*, 10.1061/(ASCE)0733-9445(1988)114:9(2085), 2085–2108.

Baji, H., Ronagh, H. R., Shayanfar, M. A., and Barkhordari, M. A. (2012). "Effect of second order analysis on the drift reliability of steel buildings." *Adv. Struct. Eng.*, 15(11), 1989–1999.

Berding, D. C. (2006). "*Wind drift design of steel framed buildings: An analytical study and a survey of the practice.*" Master's thesis, Virginia Polytechnic Institute and State Univ., Blacksburg, VA.

Bernal, D. (1998). "Instability of buildings during seismic response." *Eng. Struct.*, 20(4–6), 496–502.

Goto, Y., and Chen, W. F. (1987). "Second-order elastic analysis for frame design." *J. Struct. Eng.*, 10.1061/(ASCE)0733-9445(1987)113:7(1501), 1501–1519.

Gupta, A., and Krawinkler, H. (2000). "Dynamic P-delta effects for flexible inelastic steel structures." *J. Struct. Eng.*, 10.1061/(ASCE)0733-9445(2000)126:1(145), 145–154.

*HR_DAD version 2.0* [Computer software]. National Institute of Standards and Technology, Gaithersburg, MD.

Humar, J., Mahgoub, M., and Ghorbanie-Asl, M. (2006). "Effect of second-order forces on seismic response." *Can. J. Civ. Eng.*, 33(6), 692–706.

LeMessurier, W. J. (1976). "A practical method of second order analysis. Part 1: Pin-jointed frames." *Eng. J.*, 13(4), 89–96.

LeMessurier, W. J. (1977). "A practical method of second order analysis. Part 2: Rigid Frames." *Eng. J.*, 14(2), 49–67.

MacRae, G. A. (1993). *P-delta design in seismic regions*, Univ. of California, San Diego.

Matsumoto, M., Ishizakia, H., Matsuokab, C., Daitoc, Y., Ichikawaa, Y., and Shimaharaa, A. (1998). "Aerodynamic effects of the angle of attack on a rectangular prism." *J. Wind Eng. Ind. Aerodyn.*, 77–78(1), 531–542.

Melbourne, W. H. (1980). "Comparison of measurements on the CAARC standard tall building model in simulated model wind flows." *J. Wind Eng. Ind. Aerodyn.*, 6(1), 73–88.

Newmark, N. M., and Rosenblueth, E. (1971). *Fundamentals of earthquake engineering*, Prentice Hall, Englewood Cliffs, NJ.

Park, S., and Yeo, D. (2016). "Database-assisted design and second-order effects on the wind-induced structural behavior of high-rise buildings." *NIST Technical Note 1940*, National Institute of Standards and Technology, Gaithersburg, MD.

Rutenberg, A. (1981). "A direct P-delta analysis using standard plane frame computer programs." *Comput. Struct.*, 14(1–2), 97–102.

*SAP 2000 version 17* [Computer software]. Computers and Structures, Inc., Berkeley, CA.

Simiu, E. (2011). *Design of buildings for wind: A guide for ASCE 7-10 standard users and designers of special structures*, 2nd Ed., Wiley, Hoboken, NJ.

Simiu, E., Gabbai, R. D., and Fritz, W. P. (2008). "Wind-induced tall building response: A time-domain approach." *Wind Struct.*, 11(6), 427–440.

Tremblay, R., Léger, P., and Tu, J. (2001). "Inelastic seismic response of concrete shear walls considering P-delta effects." *Can. J. Civ. Eng.*, 28(4), 640–655.

Venanzi, I. (2005). "Analysis of the torsional response of wind-excited high-rise building." Ph.D. dissertation, Universita degli Studi di Perugia, Perugia, Italy.

White, D. W., and Hajjar, J. F. (1991). "Application of second-order elastic analysis in LRFD: research to practice." *Eng. J.*, 28(4), 133–148.

Williamson, E. (2003). "Evaluation of damage and P-Δ effects for systems under earthquake excitation." *J. Struct. Eng.*, 10.1061/(ASCE)0733-9445(2003)129:8(1036), 1036–1046.

Wilson, E. L., and Habibullah, A. (1987). "Static and dynamic analysis of multi-story buildings, including P-delta effects." *Earthquake Spectra*, 3(2), 289–298.

Wood, B. R., Beaulieu, D., and Adams, P. F. (1976). "Column design by P-delta method." *J. Struct. Div.*, 102(2), 411–427.

Yeo, D. (2011). "Database-assisted design for high-rise structures in mixed extreme wind climate." *13th Int. Conf. on Wind Engineering*, Amsterdam, Netherlands.

Yeo, D. (2013). "Multiple points-in-time estimation of peak wind effects on structures." *J. Struct. Eng.*, 10.1061/(ASCE)ST.1943-541X.0000649, 462–471.